Wall effects for spherical particle in confined shear-thickening fluids

Tian, Shuai

DOI:
10.1016/j.jnnfm.2018.03.010

Document Version
Peer reviewed version

Citation for published version (Harvard):
Tian, S 2018, 'Wall effects for spherical particle in confined shear-thickening fluids', *Journal of Non-Newtonian Fluid Mechanics*, vol. 257, pp. 13-21. https://doi.org/10.1016/j.jnnfm.2018.03.010

Wall effects for spherical particle in confined shear-thickening fluids

Shuai Tian

PII: S0377-0257(17)30511-6
DOI: 10.1016/j.jnnfm.2018.03.010
Reference: JNNFM 3989

To appear in: *Journal of Non-Newtonian Fluid Mechanics*

Received date: 8 November 2017
Revised date: 7 March 2018
Accepted date: 14 March 2018

Please cite this article as: Shuai Tian , Wall effects for spherical particle in confined shear-thickening fluids, *Journal of Non-Newtonian Fluid Mechanics* (2018), doi: 10.1016/j.jnnfm.2018.03.010

Hightlights

- Wall effects for spherical particle in shear-thickening fluids were studied.
- Drag coefficient decreases with increase in Reynolds number.
- Relation between drag coefficient and flow behaviour index was studied and explained.
- Length of recirculation wakes under various conditions was given.
- Influence may be neglected if wall is far enough from the particle

WALL EFFECTS FOR SPHERICAL PARTICLE IN CONFINED SHEAR-THICKENING FLUIDS

Shuai Tian[1,2*]

1. School of Energy and Power Engineering, Shandong University, Jinan, Shandong, 250061, China

2. School of Chemical Engineering, University of Birmingham, Edgbaston, B15 2TT, United Kingdom

*****Author to whom correspondence should be addressed: Email: tsh19850227@163.com;

Abstract

Flow past rigid sphere in cylindrical tubes filled with shear-thickening power law fluids is simulated by Computational Fluid Dynamic (CFD) model in steady-state mode with fixed computational domain. The CFD model is validated with previous researchers' work for Newtonian and shear-thinning power law rheologies in both bounded and unbounded mediums. New simulations are executed over flow conditions of Reynolds number, Re: $0.001 \le \mathrm{Re} \le 100$, diameter ratio, λ (diameter of tube to that of particle, $\lambda = D/d$): $2 \le \lambda \le 50$, and flow behaviour index, n: $1 \le n \le 1.8$. Wall effects on flow patterns and drag phenomena are investigated and found to be functions of Reynolds number, diameter ratio and flow behaviour index. Numerical results reveal that drag coefficient decreases with the increase in Reynolds number. Contribution on the drag coefficient from pressure force drops with increasing flow behaviour index, and is generally smaller than that from friction force. Length of recirculation wake increases with enhancement in flow behaviour index in the case of less severe wall effects. Wall effects on flow can be neglected if the wall is far enough from the particle.

Keywords: CFD; wall effects; shear-thickening fluids; drag coefficient

1. Introduction

The sedimentation motion of particles in liquids or flow past rigid bodies is of great interest in theoretical and experimental studies due to its high demand in a wide range of applications, such as gravity-based solid-liquid separator, transportation of particles in slurry, falling ball viscometer and fluidized bed [1, 2]. In these studies, the simplest case of single spherical particle is always providing fundamental and essential understanding on more complex cases. Typical intricate examples include those of particles with non-spherical shape (e.g. cubes [3], cylinders [4], oblates [5]); multi-particles system [6, 7] or surrounding fluids with unsteady motion [8-10]. For single particle cases, the interaction between particle and fluid is determined by a large number of variables, including size and density of the particle, density and rheological properties of fluids, as well as the diameter of the tube in the case of bounded flow. However, the drag force, F_D (or in dimensionless forms, such as drag coefficient, C_D or its correction factor, Y) obtains the most attention from researchers.

Considerable work has been devoted to revealing the standard drag curve for over one century and abundant results are available in literatures with infinite mediums. Stokes [11] solved the partial differential equation by ignoring inertial effects and obtained the analytical solution for solid sphere in Newtonian fluids under creeping flow condition (i.e. $Re << 1$). However, for flow at large distance from the sphere or at high Reynolds number, creeping flow approximation is not satisfied. Oseen [12] simplified, rather than neglected, the inertial terms and achieved analytical solution with an additional term on Stokes' form. Furthermore, by fully taking into account the inertia, solutions were given in series expansion (e.g. second order by Proudman and Pearson [13]; third order by Chester and Breach [14]) at low Reynolds number region ($< \sim 4$). Later, Liao [15] utilized "Homotopy Analysis Method" to deal with the non-linear term in N-S equations and achieved solution for flow with Re up to 30. Due to the difficulty of solving partial differential equations, numerical approaches were employed for this problem as well. LeClair, et al. [16] worked out the drag on sphere for $Re = 0.01 – 400$ using finite difference method. Later, Fornberg [17] assessed recirculation wake structure and calculated the drag coefficient with Newton's method for a much larger range of Re (up to 5000).

Invesitigations with non-Newtonian power law rheologies can be categorized into shear-thinning and shear-thickening. For pseudoplastic types, Wasserman and Slattery [18] obtained the upper and lower

predictions on the drag coefficient correction factor with the application of variational principle. Subsequently, Cho and Hartnett [19] improved Wasserman and Slattery's solution by providing a closer upper-lower bound at low values of flow behaviour index, n (< ~ 0.8). The drag in power law fluids was also estimated by different numerical techniques, such as finite-element method [20, 21]; finite-volume based method [22]. Studies on dilatants fluids are not so much as those on shear-thinning fluids, Tripathi and Chhabra [23] numerically estimated the values of C_D for Re from 0.001 to 100 and n from 1.0 to 1.8. However, their work was proven to be inaccurate at high Reynolds number and has been improved in following extensive numerical study of Dhole, et al. [22]. More complete review can be found in books [24-26].

In contrast to the unbounded fluids in the theoretical studies, practical problems in engineering applications are always investigated in finite-size containers. With the presence of confining walls, the motion of particle is retarded, i.e. C_D decreases comparing with that in unbounded fluids. Considering a tube with cylindrical boundary, retardation effect of the wall results from the flow flux in the opposite direction to the motion of particle along the axis. In the literatures, for Newtonian fluids, wall effects were analytically studied in the creeping flow region for $0 < 1/\lambda \le 0.8$ [27, 28]. Beyond creeping flow region, Wham, et al. [29] utilized finite element method to treat the flow and developed a drag correlation for Re up to 100 and $1/\lambda$ from 0.08 to 0.7. Wham et al.'s work was subsequently extended to Re = 200 by Kishore and Gu [30] for $2 \le \lambda \le 30$. They employed commercial CFD software and obtained a correlation for drag coefficient with an average error of ± 9.2%. For power law fluids, Gu and Tanner [20] simulated the flow with n from 0.1 to 1 and concluded that wall effects could be negligible for $n \le 0.5$ under creeping flow condition. Missirlis, et al. [31] studied the wall effects and listed drag coefficient correction factor Y over wide ranges of n from 0 to 1, and λ from 2 to 50 using both finite-element and finite-volume methods. Song, et al. [32] provided detailed documentation on wake characteristics and drag coefficient under the influence of tube wall with the help of COMSOL.

Unlike abundance of work with Newtonian and shear-thinning power law fluids, focus on the wall effects in shear-thickening fluids is very rare. Recently, Rajasekhar and Kishore [33] reported their work on confined spherical particle in shear-thickening fluids of n = 1.0 – 1.8. Although an excellent agreement with literatures was claimed, as incorrect calculation was used to validate the model, some inaccuracies were shown in their results. For example, drag coefficient differed by a factor of ~ 2 with Newtonian fluids, comparing with other

peers' work [29, 31]. In present study, new results on the wall effects for a spherical particle in shear-thickening fluids are reported, showing ~200% – ~400% differences on the drag coefficient from those reported by Rajasekhar and Kishore [33]. Meanwhile, flow conditions considered here are λ = 2 – 50 and Re = 0.001 – 100, greatly extended those, λ = 2 – 5 and Re = 1 – 100 used by Rajasekhar and Kishore [33].

2. Theory

2.1. Rheological model

The fluids used in this study are assumed to be incompressible with constant density of ρ_F and rheologically time-independent. The non-Newtonian power law model is described by Eq. (1):

$$\tau = k\dot{\gamma}^n \tag{1}$$

where *??* is the shear stress and *k* is the fluid consistency index. Thus, the apparent viscosity η is given by:

$$\eta = k\dot{\gamma}^{n-1} \tag{2}$$

For shear-thinning (pseudoplastic) fluids, $n < 1$, and for shear-thickening (dilatant) fluids, $n > 1$. For $n = 1$, the model corresponds to Newtonian behaviour with a shear-independent viscosity μ (i.e. $\mu = \eta$).

2.2. Reynolds number

For a spherical particle in power law fluids, the Reynolds number is given by

$$\mathrm{Re} = \frac{\rho_F V^{2-n} d^n}{k} \tag{3}$$

where *V* is the relative velocity between particle and tube wall, *d* is the diameter of particle.

2.3. Drag coefficient

For convenience, the drag of particle is assessed using its dimensionless form, drag coefficient, C_D, expressed as

$$C_D = \frac{F_D}{\frac{1}{2}\pi r^2 \rho_F V^2} \tag{4}$$

where F_D is the drag force acting on the particle, r is the radius of particle. For rigid particle, C_D consists of two parts, C_f from friction and C_p from pressure [24], i.e.

$$C_D = C_f + C_p \tag{5}$$

Specially under creeping flow condition, drag force in Newtonian fluids can be worked out by Stokes' formula [11],

$$F_D = 6\pi r \mu V \tag{6}$$

In power law fluids, the drag force can be computed from Eq. (6) by introducing a dimensionless number, drag coefficient correction factor, Y, as

$$F_D = 6\pi r \eta V Y \tag{7}$$

where η is calculated by assuming the characteristic shear rate around the sphere to be equal to V/d [24]. Considering Eqs. (3) (4) (7), the drag coefficient correction factor, Y can be expressed in a simpler and more popular form:

$$Y = \frac{\mathrm{Re} C_D}{24} \tag{8}$$

By substituting $Y = 1$, Eq. (7) reduces to Stokes' formula (i.e. Eq. (6)), and Eq. (8) leads to relation of $C_D = \frac{24}{\mathrm{Re}}$ for Newtonian rheologies in creeping flow region.

2.4. Governing equations

The governing transport equations for this study are continuity and momentum equations which can be written in their general forms [34], as:

Continuity: $$\nabla \cdot U = 0 \quad (9)$$

Momentum: $$\rho_F \frac{DU}{Dt} = -\nabla p + \nabla \eta\dot{\gamma} \quad (10)$$

where p is fluid pressure, $\boldsymbol{U}$ is the velocity field and $\dot{\gamma}$ is the second invariant of the rate-of-strain tensor, defined as $\dot{\gamma} \equiv \left[\frac{1}{2}(\dot{\gamma}:\dot{\gamma})\right]^{\frac{1}{2}}$.

3. CFD Simulations

The commercial software package of ANSYS Workbench 16.0 was ultilised to set up and execute the simulations. The flow geometries were generated and meshed in the software ICEM, while flow was specified, solved and post-processed using CFX 16.0. The original geometries were a series of straight tubes with varying diameters, together with one sphere symmetrically placed at the tube centre. By implementing axisymmetric configuration, original geometries were simplified to quasi two-dimensional model, achieved by sweeping 1° with a 2D mesh. Each simplified geometry consists of five boundaries: inlet, outlet, symmetry, tube wall and particle wall, as depicted in Fig. 1. The entrance length, L_{in} and exit length, L_{out} were chosen as $L_{in} = L_{out} = 99r$ to eradicate inlet and outlet boundary effects.

All geometries used here were meshed with hexahedral cells. To optimise the mesh size, it is necessary to carry out a mesh-independence study for reliable results, meanwhile keeping computational loads as low as possible. This was done by performing a number of simulations with different mesh sizes, starting from a coarse mesh and refining it until results were no longer dependent on the mesh size. For each mesh achieved with varying diameters, the mesh size near particle wall was progressively reduced down to $0.06r$ to enhance mesh resolution in this region where high velocity gradients exist (as depicted in Fig. 2). The quality of every mesh, used in present study, measured by its orthogonality and warpage was over 0.85, well above the generally accepted minimum value of 0.4 for a good mesh.

To discretise the governing transport Eqs. (9), (10), the CFX code uses a finite-volume-based method. In this

method, the variable value, ϕ_{ip} is calculated at an integration point, from the variable value at the upwind node, ϕ_{up}, and the variable gradient, $\nabla\phi$, thus

$$\phi_{ip} = \phi_{up} + \beta\nabla\phi\Delta\mathbf{r} \tag{11}$$

where β is a blend factor and $\Delta\mathbf{r}$ is the vector from the upwind node to the integration point. First order accurate scheme is obtained with $\beta = 0$. This scheme is robust, but may introduce discretisation error. On the other hand, second order accurate scheme is obtained with $\beta = 1$. This scheme is unbounded and may result in non-physical values. A so-called 'High Resolution Advection Scheme' was implemented in present study and the value of β is computed locally to be as close to 1 as possible, intending to satisfy the requirements of both accuracy and boundedness [35].

Model used in present work is with stationary flow domain and simulations were conducted in the steady-state mode. Uniform velocities were specified at the inlet, and zero gauge pressure condition was set at the outlet. In contrast to that used in most literatures [21-23, 33], the inlet velocities and no-slip condition were assigned at the tube wall, as work of Missirlis, et al. [31]. Particle wall was specified as stationary and no-slip.

Numerical solutions were assumed when the root mean square (RMS) of both mass and momentum residuals reached a convergent target of 10^{-6} which is accepted as a good level of accuracy. In fact, however, even lower RMS residual values were generally reached by most of the equations. Special study has been done and it could be confirmed that the results reported below would not change with smaller specified target of RMS residual. Achieving this level of convergence typically required 50 – 200 iterations.

4. Validation of CFD Model

CFX is a widely used code and has been proven to be generally stable and reliable. However, to maximize my confidence, validations were conducted here as much as possible by comparing present work with literatures. Two groups of validations, simulating flow with both unbounded and bounded fluids were carried out and described as below.

4.1. Validations in unbounded Newtonian and shear-thickening fluids.

First group of validations were carried out by simulating flows with Re from 0.001 to 100, n from 1.0 to 1.8 and λ from 2 to 50. Then results for $\lambda \to \infty$, which corresponded to unbounded condition were worked out by extrapolating data collected from λ = 2 to 50. As drag coefficient listed in Table 1, in the region of Re = 0.001 – 1, present results show an excellent agreement in comparison with previous work [22, 23]. At Re = 10 and 100, results still greatly agree with Finite-difference method (FDM) in Dhole et al. [22], but slightly deviate from Finite-volume method (FVM) with a maximum difference of ~ 6.2%, which is still at an acceptable level.

4.2. Validations in bounded Newtonian and shear-thinning fluids.

Second group of validations were with confined particle in Newtonian and shearing-thinning fluids for λ from 2 to 50. Under creeping flow condition (Re = 0.001), a maximum difference of ~ 1.2% is shown in comparisons of drag correction factor, Y in Table 2 for both Newtonian and shear-thinning fluids. At moderate Reynolds numbers, as shown in Table 3 for Newtonian fluid present results differ by ~ 15% from Wham et al. [29]'s work while Re = 10 and λ = 10. However, the agreement is still great in comparisons with other combinations of Re and λ. Results presented in the work of Rajasekhar and Kishore [33] with λ = 5 are also cited in Table 3, showing differences of ~ 96% at Re = 1 and up to ~ 124% at Re = 100 from present work. For a power law fluid of n = 0.4, predicted results were compared with literature [32] in term of normalised drag coefficient, which was normalised by the corresponding values in Newtonian fluids at same λ and Re. Good consistency is shown at Re = 1, 10 and 100, respectively, as indicated in Table 4.

In summary, although some slight difference exists, given the generally excellent agreement in the validations above, it is believed that the present CFD model is sufficiently robust and reliable for the purpose of studying the wall effects for spherical particle in confined shear-thickening fluids.

5. Results and discussion

Flow patterns and drag phenomena are assessed in functions of Reynolds number, Re; diameter ratio, λ and flow behaviour index, n.

5.1. The effect of Reynolds number on flow patterns and drag phenomena.

In Fig. 3, drag coefficient is plotted as a function of Reynolds number on log-log coordinate. It can be seen that

C_D is dependent on Re in a similar way for n from 1.0 to 1.8 and λ from 2 to 50. C_D decreases with the increase in Re throughout the ranges of λ and n. With given n and λ, C_D is inversely proportional to Re at small values of Reynolds number. Take case of n = 1.8 and λ = 50 as an example, inverse relation is satisfied by C_D and Re for Re up to ~ 0.1, and it is generally interpreted as a feature of creeping flow [24]. Further insight into the effect of Reynolds number on flow is carried out by examining the streamline patterns. Fig. 4 presents streamlines of flow past a spherical particle for shear-thickening fluid of n = 1.8 from Re = 0.001 to 100. It can be observed that streamlines are almost symmetrical before and after the particle until Re = 0.1, corresponding to the inverse relation between C_D and Re. While Re is increasing, the drag is greatly affected by the inertial force. The fore-and-aft symmetric characteristics of streamline patterns gradually disappears, and at Re = 100, clear recirculation wake can be seen after the particle. Focus back to drag coefficient, as shown in Fig. 3, C_D starts to deviate from the inverse relation with Re at Re = ~ 0.1, denoting the development from creeping flow to non-creeping flow. The contributions of pressure drag coefficient C_p and friction drag coefficient C_f to total drag coefficient C_D are also presented in Fig. 3 in form of C_p/C_f. It can be concluded that C_f makes the dominate contribution from the fact that C_p/C_f is generally below unity. In the region of Re = 0.001 – ~ 1, C_p/C_f is independent of the value of Reynolds number. However, with the increase in Re, C_p/C_f shows exponential growth and reaches its maximum value at Re = 100.

5.2. The effect of diameter ratio on flow patterns and drag phenomena.

Wall effects are yielded by the backward flux of the fluid displaced by the particle. The diameter ratio indicates the extent of wall effects, the closer to unity the diameter ratio, the severer is the influence from the wall. Drag coefficient C_D is depicted as a function of diameter ratio λ at Re = 0.001 in Fig. 5 and Re = 100 in Fig. 6, respectively (values of drag correction factor Y are listed in Table 5 for quantitive examination). Qualitatively similar trend is observed for curves with varying values of n. As the diameter ratio is increasing, the effects from the wall diminish and finally disappear. Starting from λ = 2, C_D decreases rapidly with the rise in λ and starts to level off beyond λ = ~ 20 under creeping flow condition (Re = 0.001), or λ = ~ 10 under non-creeping flow condition (Re = 100). Finally, drag coefficient converges to its values in unbound fluids respectively (i.e. C_D reaches constant while $\lambda \to \infty$). Similar phenomena are observed in the comparison of wakes with varying diameter ratios. As shown in Fig. 7, for both n = 1.0 and 1.8, the wakes progressively grow while the wall is moving outward to the particle. At λ = 10, length of recirculation wake (defined as the length along the axis of tube) reaches 1.72r for n = 1.0, and 1.94r for n = 1.8, respectively and does not change with further departure of

wall from particle beyond λ = 10. It is possibly worth to mention here that as the inaccuracy issue, recirculation wake could not be observed at Re = 100 with λ = 2 by Rajasekhar and Kishore [33] and was attributed to the wall effects in their conclusion. Ratio of flow rate recirculating in the envelope (Q_W) to the main flow rate at inlet (Q_B), expressed as a percentage, is also given in Fig. 7. As expected, increasing λ results in a rise in Q_B, thus, lowering the value of Q_W/Q_B (while $\lambda \to \infty$, Q_W/Q_B tends to be zero). Length of recirculation wakes and percentage of recirculation flow rate at Re = 100 over ranges of n = 1.0 – 1.8 and λ = 2 – 50 is summarised in Table 6 and Table 7, respectively.

5.3. The effect of flow behavior index on flow patterns and drag phenomena.

The flow behaviour index n is a measure of the degree of non-Newtonian behaviour; the greater the departure from unity, the more pronounced are the non-Newtonian properties of the fluid. As shear rate increases, shear-thickening rheology behaves more viscous than Newtonian fluid. While fluid flows past the particle, the additional shear yielded by the particle surface results in a rise in apparent viscosity, thus retarding the flow near the particle. Fig. 8 displays ten contours of velocity field which is normalised by the uniform inlet velocity for n = 1.0 – 1.8 and λ = 2; 15 under creeping flow condition (Re = 0.001). Low normalised velocity field is formed around the particle, while high normalised velocity field is formed beside the particle. From Fig. 5, it can be found that for a given combination of Re and λ, shear-thickening rheologies results in larger low normalised velocity field and greater velocity deviation over Newtonian medium. In contrast to velocity field, comparison of recirculation wakes with different values of n looks more complex. Generally, the formation and growth of wake is prompted by relatively low velocity behind particle and relatively high velocity beside particle. As shown in Fig. 9, for λ = 15, at Re = 100, flow with n = 1.8 contributes the longest recirculation wake length, which is in accordance with previous peers' work [24]. However, for λ = 2, opposite phenomenon is observed that the length of the wake tends to be shorter due to the dilatant properties of the fluid. This counterintuitive phenomenon may be attributed to the strong impact of the wall: 1, additional shear is imposed by the relative motion between fluid and the wall, then retards the side flow; 2, high radial velocity of fluid is generated from the dramatic change in cross-section, and then affects the formation of wake behind the particle. Such high radial velocity also influences recirculation flow rate. As indicated in Fig. 9, for λ = 2, under severe wall effects, Q_W/Q_B with Newtonian fluid is ~ 6.2 times larger than that with shear-thickening fluids (n = 1.8). However, rate of recirculation flow tends to be independent of flow behaviour index with increase in λ, e.g. for λ = 50, percentage of recirculating flow rate is identically 0.0009% over range of n = 1.0 – 1.8 (shown in Table 7).

Conclusions on the comparison of drag coefficient with different values of n are not explicit. As shown in Fig. 3, for λ = 2, throughout the range of Re, Newtonian fluid yields the smallest C_D, comparing with shear-thickening types; for λ = 5, all these five curves converge and it is difficult to distinguish which rheology contributes the largest drag; for each case of λ > 5, a crossover of C_D could be seen between Re = 1 and 10, and on the two sides of this point, opposite results are obtained. Under creeping flow condition (Re = 0.001), the crossover of C_D is at λ = ~5 (shown in Fig. 5), which is consistent with that for shear-thinning power law fluids [31]. With the increase in Reynolds number, as shown in Fig. 10, the corresponding diameter ratio of crossover of C_D shifts from λ = ~5 at Re = 1 to λ = ~10 at Re = 7, and finally disappears at Re = 10 (depicted in Fig. 3). As the flow condition of λ > 5 was not covered, such intricate phenomenon was not observed in the work of Rajasekhar and Kishore [33], and is believed to result from the quantitative values of dimensionless shear rate ($\dot{\gamma}/(V/d)$) around the particle surface. At a given Reynolds number, Newtonian rheology leads to a larger value of C_D (Y) if dimensionless shear rate is smaller than 1, or a smaller value of C_D (Y) if $\dot{\gamma}/(V/d)$ is larger than 1, comparing with shear-thickening fluids. In present study, under the condition(s) of Re is high enough or/and additional shear from wall is sufficient (i.e. λ is small), dimensionless shear rate is greater than 1 in most area. Therefore, C_D is larger for shear-thickening fluids than Newtonian fluids. On the other hand, at small values of Re and with large λ, flow is more likely to be less sheared by the particle, thus leading to a low drag coefficient by shear-thickening properties. In Fig. 3, C_p/C_f displays qualitatively similar trend for all diameter ratios throughout the range of Re. As the value of n increases, friction force acting on particle increases, thus resulting less contribution from pressure drag.

6. Conclusions

Flow past spherical particle in cylindrical tubes filled with shear-thickening power law fluids was simulated by CFX with validated CFD model for wide ranges of Reynolds number, diameter ratio and flow behahiour index. Total drag coefficient is determined by Re, λ and n in following relations: 1, C_D decreases with the increase in Re thoroughly; 2, C_D declines with increasing λ until the wall effects are negligible; 3, C_D drops with increasing n under condition of small Re and large λ, but increases under condition(s) of large Re or/and small λ. While Re is increasing from 0.001, C_p/C_f keeps constant and goes up exponentially beyond Re = ~ 1. In most cases of this study, friction offers more drag than pressure for Newtonian fluids, however, even more for shear-thickening fluids. At high Reynolds number, recirculation wake may form after the particle. Length of wake increases as diameter ratio rises until wall effects disappear. Generally,

shear-thickening properties tend to shorten the wake length. This conclusion, however, may vary under severe wall effects.

Acknowledgements

This research did not receive any specific grant from funding agencies in the public, commercial, or not-for-profit sectors.

Nomenclature

C_D Total drag coefficient, -

C_f Friction drag coefficient, -

C_p Pressure drag coefficient, -

d Particle diameter, m

D Tube diameter, m

F_D Total drag force, N

k Fluid consistency index, Pa s^n

n Flow behavior index, -

r Particle radius, m

R Tube radius, m

Re Reynolds number, -

t Time, s

V Relative velocity between particle and tube wall, m s^{-1}

Y Drag coefficient correction factor, -

Greek symbols

$\dot{\gamma}$ Shear rate, s^{-1}

η Apparent viscosity, Pa s

λ Diameter ratio or radius ratio, D/d or R/r, -

μ Viscosity for Newtonian fluid, Pa s

ρ_F Density of fluid, kg m^{-3}

ρ_P Density of particle, kg m^{-3}

τ Shear stress, Pa

References

[1] A.A. Gavignet, I.J. Sobey, Model aids cuttings transport prediction, J. Petrol. Technol., 41 (1989) 916-921.
[2] Y. Li, E. Kuru, Numerical modelling of cuttings transport with foam in horizontal wells, J. Can. Pet. Technol., 42 (2003) 54-61.
[3] N. Agarwal, R.P. Chhabra, Settling velocity of cubes in Newtonian and power law liquids, Powder Technol., 178 (2007) 17-21.
[4] I.E. Kareva, V.L. Sennitskii, Motion of a circular cylinder in a vibrating liquid, J. Appl. Mech. Tech. Phys., 42 (2001) 276-278.
[5] A. Tripathi, R.P. Chhabra, Hydrodynamics of creeping motion of an ensemble of power law fluid drops in an immiscible power law medium, Int. J. Eng. Sci., 32 (1994) 791-803.
[6] M. Kogan, L. Ducloué, J. Goyon, X. Chateau, O. Pitois, G. Ovarlez, Mixtures of foam and paste: suspensions of bubbles in yield stress fluids, Rheol. Acta, 52 (2013) 237-253.
[7] O. Merkak, L. Jossic, A. Magnin, Spheres and interactions between spheres moving at very low velocities in a yield stress fluid, J. Non-Newton. Fluid, 133 (2006) 99-108.
[8] T. Sarpkaya, Forces on cylinders and spheres in a sinusoidally oscillating fluid, J. Appl. Mech., 42 (1975) 32-37.
[9] V.L. Sennitskii, Motion of a sphere in a vibrating liquid in the presence of a wall, J. Appl. Mech. Tech. Phys., 40 (1999) 662-668.
[10] J.A. Weinstein, The motion of bubbles and particles in oscillating liquids with applications to multiphase flow in Coriolis meters, in, ProQuest, 2008.
[11] G.G. Stokes, On the Effect of the Internal Friction of Fluids on the Motion of Pendulums, Pitt Press, Pittsburgh, 1851.
[12] C.W. Oseen, Neuere Methoden und Ergebnisse in der Hydrodynamik, Akademische Verlagsgesellschaft, Leipzig, 1927.
[13] I. Proudman, J.R.A. Pearson, Expansions at small Reynolds numbers for the flow past a sphere and a circular cylinder, J. Fluid Mech., 2 (1957) 237-262.
[14] W. Chester, D.R. Breach, On the flow past a sphere at low Reynolds number, J. Fluid Mech., 37 (1969) 751-760.
[15] S.J. Liao, An analytic approximation of the drag coefficient for the viscous flow past a sphere, Int. J. Non-Linear Mech., 37 (2002) 1-18.
[16] B.P. LeClair, A.E. Hamielec, H.R. Pruppacher, A numerical study of the drag on a sphere at low and intermediate Reynolds numbers, J. Atmos. Sci., 27 (1970) 308-315.
[17] B. Fornberg, Steady viscous flow past a sphere at high Reynolds numbers, J. Fluid Mech., 190 (1988) 471-489.
[18] M.L. Wasserman, J.C. Slattery, Upper and lower bounds on the drag coefficient of a sphere in a power‐model fluid, AlChE J., 10 (1964) 383-388.
[19] Y.I. Cho, J.P. Hartnett, Drag coefficients of a slowly moving sphere in non-Newtonian fluids, J. Non-Newton. Fluid, 12 (1983) 243-247.
[20] D. Gu, R.I. Tanner, The drag on a sphere in a power-law Fluid, J. Non-Newton. Fluid, 17 (1985) 1-12.
[21] A. Tripathi, R.P. Chhabra, T. Sundararajan, Power law fluid flow over spheroidal particles, Ind. Eng. Chem. Res., 33 (1994) 403-410.

[22] S.D. Dhole, R.P. Chhabra, V. Eswaran, Flow of power-law fluids past a sphere at intermediate Reynolds numbers, Ind. Eng. Chem. Res., 45 (2006) 4773-4781.
[23] A. Tripathi, R.P. Chhabra, Drag on spheroidal particles in dilatant fluids, AlChE J., 41 (1995) 728-731.
[24] R.P. Chhabra, Bubbles, Drops, and Particles in Non-Newtonian Fluids, Second Edition, CRC Press, Boca Raton, Florida, 2006.
[25] R.P. Chhabra, J.F. Richardson, Non-Newtonian Flow in the Process Industries: Fundamentals and Engineering Applications, Butterworth-Heinemann, Oxford, 1999.
[26] R. Clift, J.R. Grace, M.E. Weber, Bubbles, Drops, and Particles, Academic Press, New York, 1978.
[27] H. Faxén, Die Bewegung einer starren Kugel längs der Achse eines mit zäher Flüssigkeit gefüllten Rohres, Arkiv foer matematik, astronomi och fysik, 17 (1923) 1-28.
[28] W.L. Haberman, R.M. Sayre, Motion of Rigid and Fluid Spheres in Stationary and Moving Liquids inside Cylindrical Tubes, in, David Taylor Model Basin Hydromechanics Lab, 1958.
[29] R.M. Wham, O.A. Basaran, C.H. Byers, Wall effects on flow past solid spheres at finite Reynolds number, Ind. Eng. Chem. Res., 35 (1996) 864-874.
[30] N. Kishore, S. Gu, Wall effects on flow and drag phenomena of spheroid particles at moderate Reynolds numbers, Ind. Eng. Chem. Res., 49 (2010) 9486-9495.
[31] K.A. Missirlis, D. Assimacopoulos, E. Mitsoulis, R.P. Chhabra, Wall effects for motion of spheres in power-law fluids, J. Non-Newton. Fluid, 96 (2001) 459-471.
[32] D.Y. Song, R.K. Gupta, R.P. Chhabra, Wall effects on a sphere falling in quiescent power law fluids in cylindrical tubes, Ind. Eng. Chem. Res., 48 (2009) 5845-5856.
[33] R.C. Rajasekhar, N. Kishore, Wall retardation effects on flow and drag phenomena of confined spherical particles in shear-thickening Fluids, Ind. Eng. Chem. Res., 51 (2012) 16755-16762.
[34] R.B. Bird, R.C. Armstrong, O. Hassager, Dynamics of Polymeric Liquids: Fluid Mechanics, Wiley, New York, 1987.
[35] T.J. Barth, D.C. Jespersen, The design and application of upwind schemes on unstructured meshes, in: 27th Aerospace Sciences Meeting, AIAA, Paper 89-0366, Reno, Nevada, 1989.

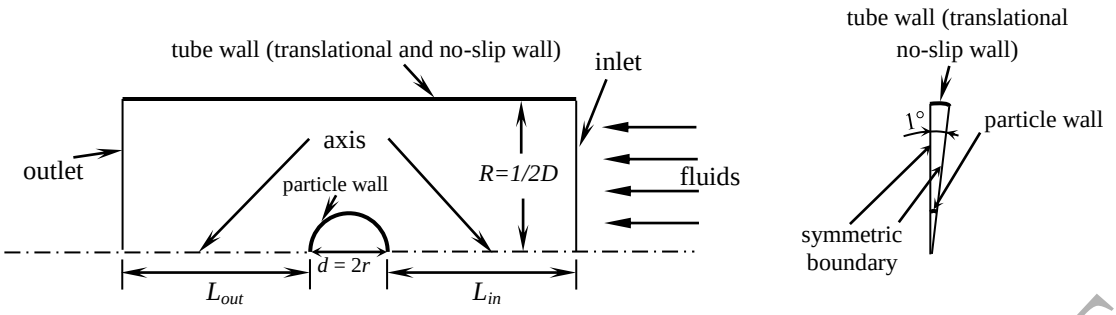

Fig. 1. Schematic representation of simplified model with boundary conditions.

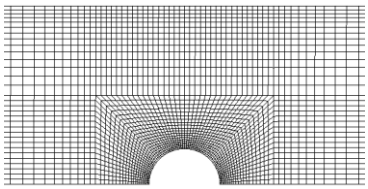

Fig. 2. Schematic of the mesh used in simulations with $\lambda = 5$.

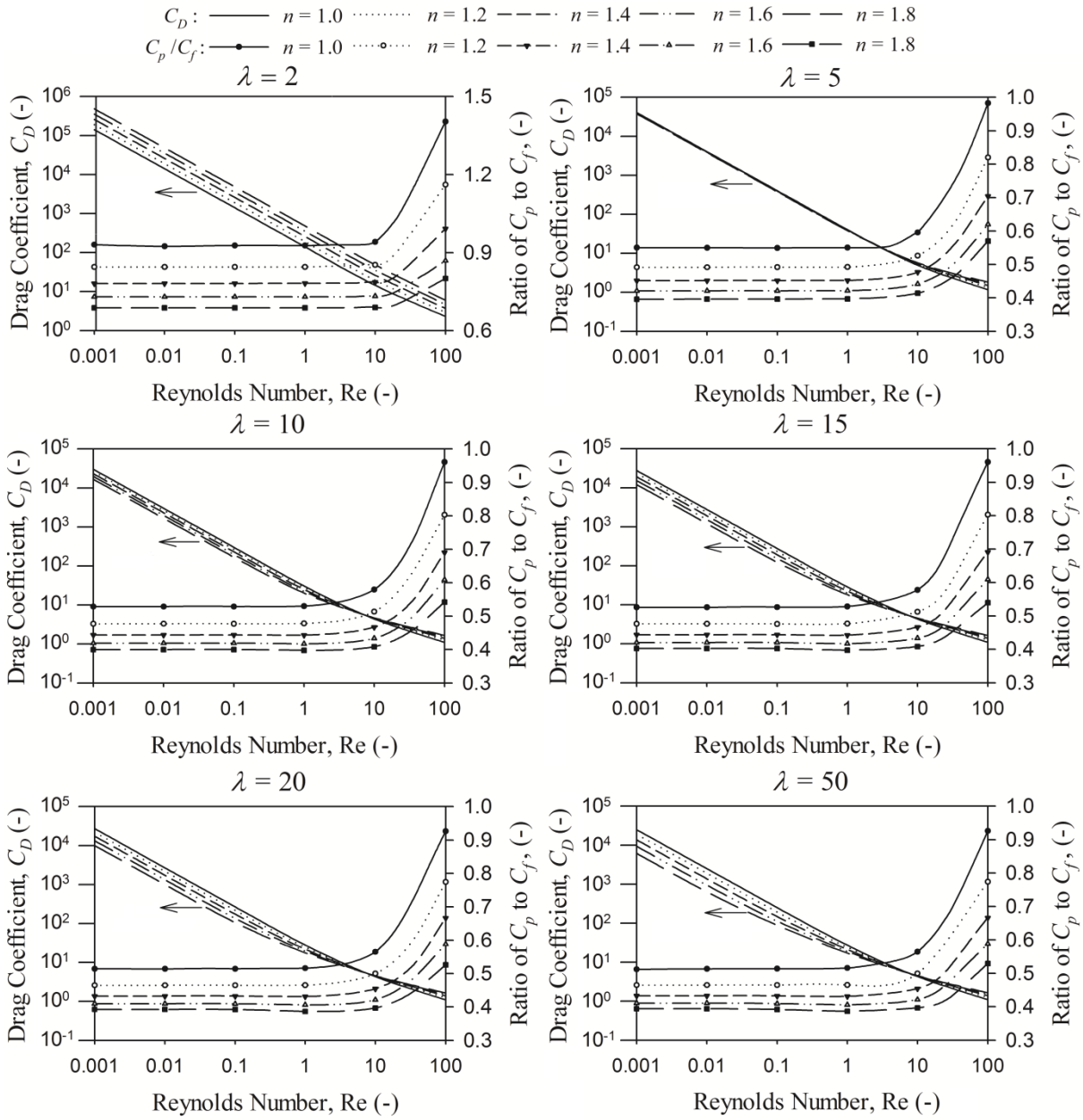

Fig. 3. Effects of Re and n on C_D and C_p/C_f with different values of λ.

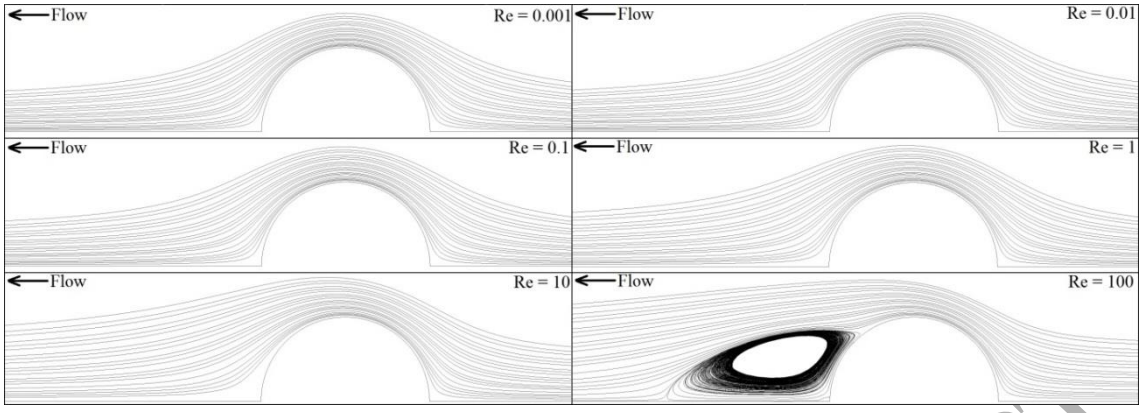

Fig. 4. Streamline patterns around the particle at Re = 0.001; 0.01; 0.1; 1; 10; 100 for shear-thickening fluid: n = 1.8 with $\lambda = 50$.

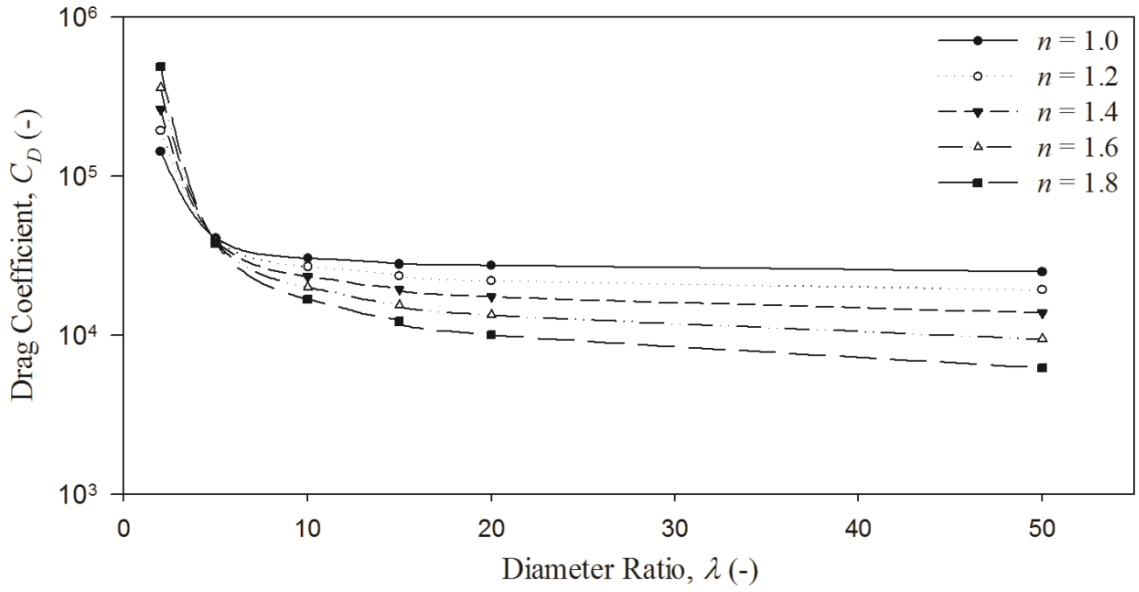

Fig. 5. Comparison of C_D with different values of λ at Re = 0.001 for Newtonian and shear-thickening power law fluids.

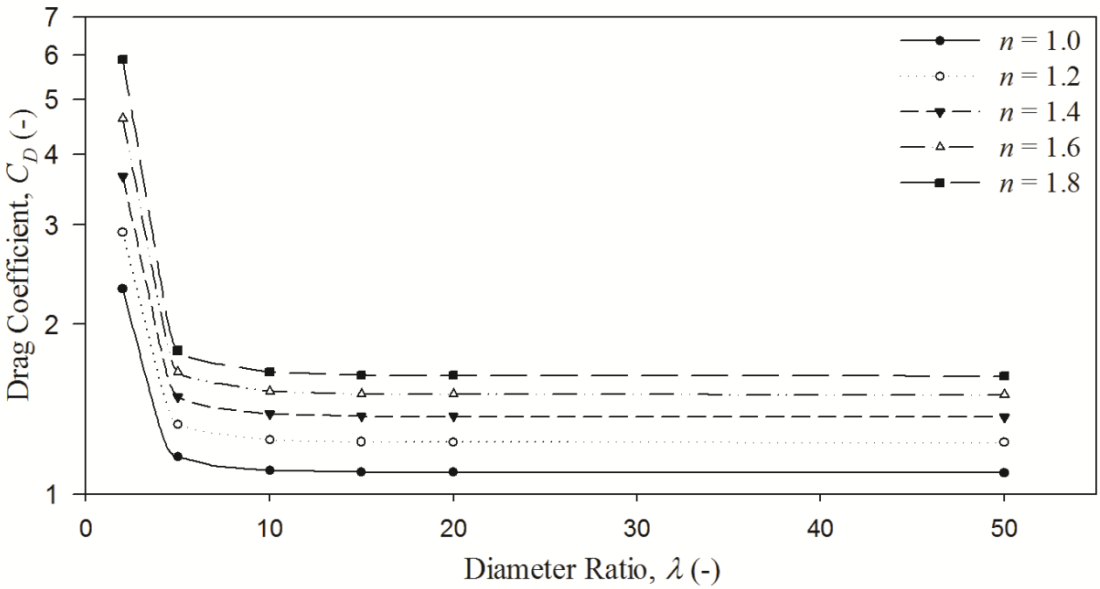

Fig. 6. Comparison of C_D with different values of λ at Re = 100 for Newtonian and shear-thickening power law fluids.

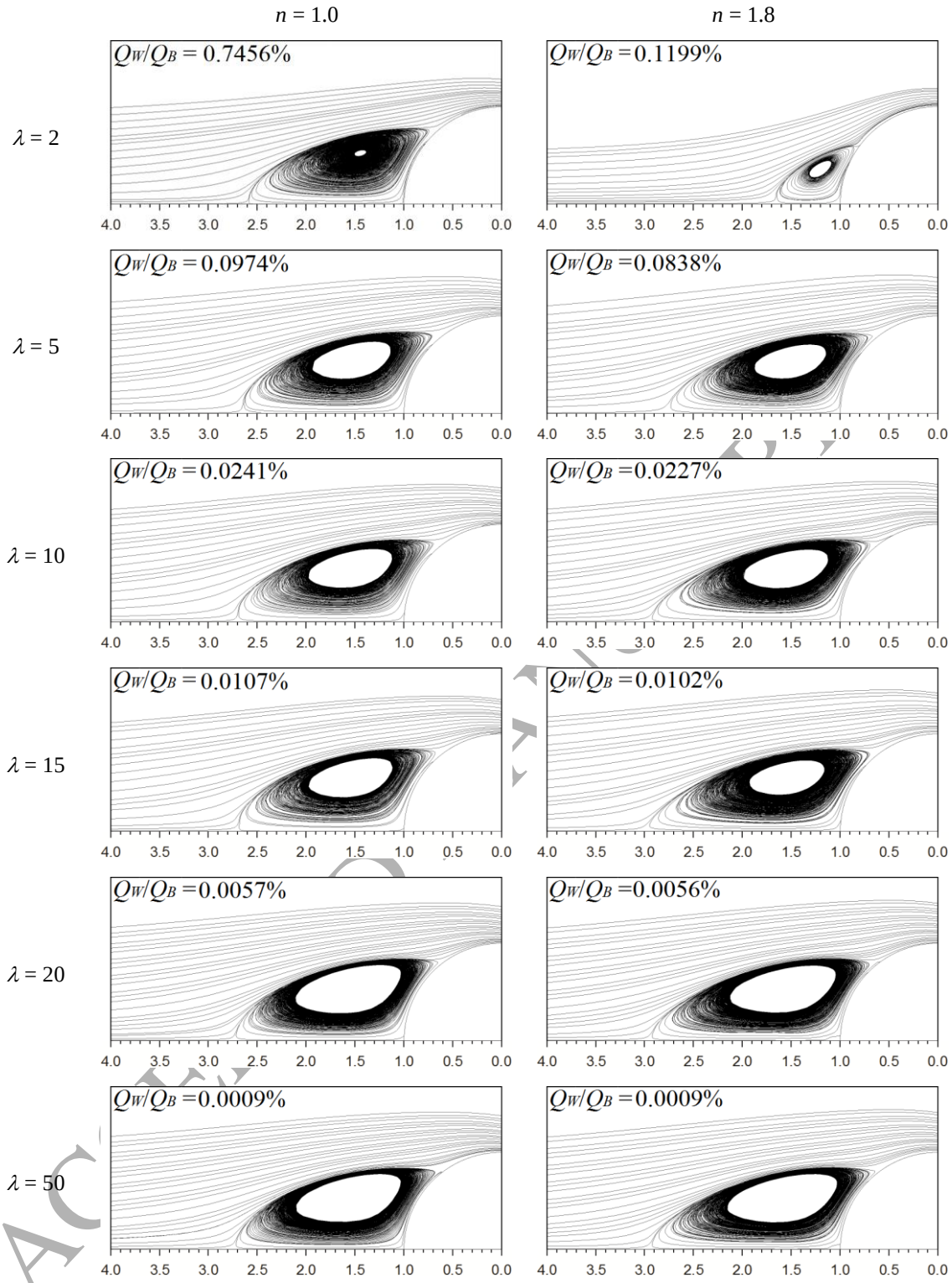

Fig. 7. Comparison of streamline patterns after the particle with different values of λ for n = 1.0 and 1.8 at Re = 100.

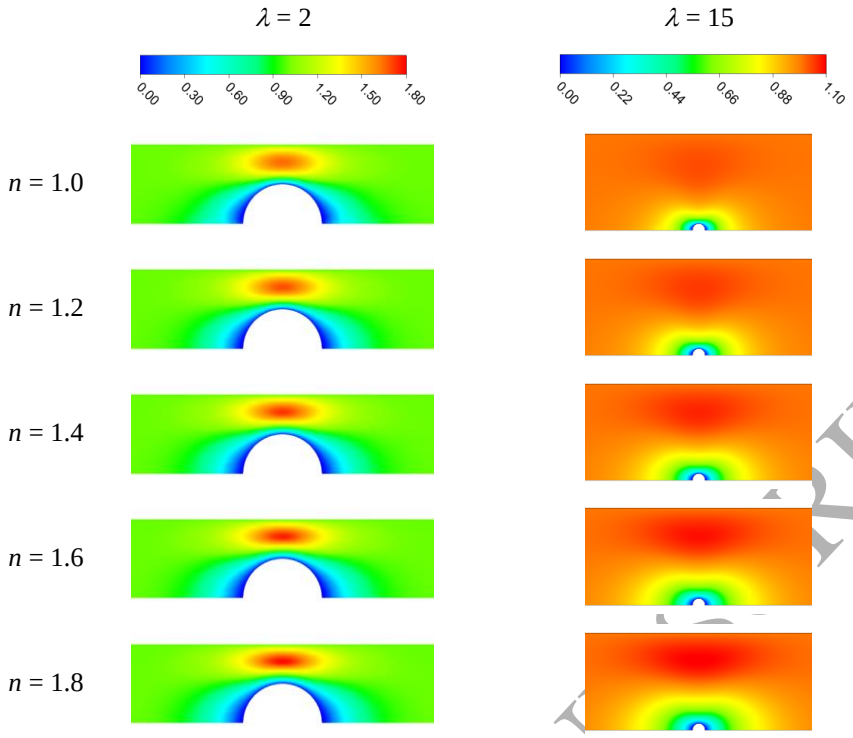

Fig. 8. Comparison of normalized velocity fields with different values of n for λ = 2 and 15 at Re = 0.001.

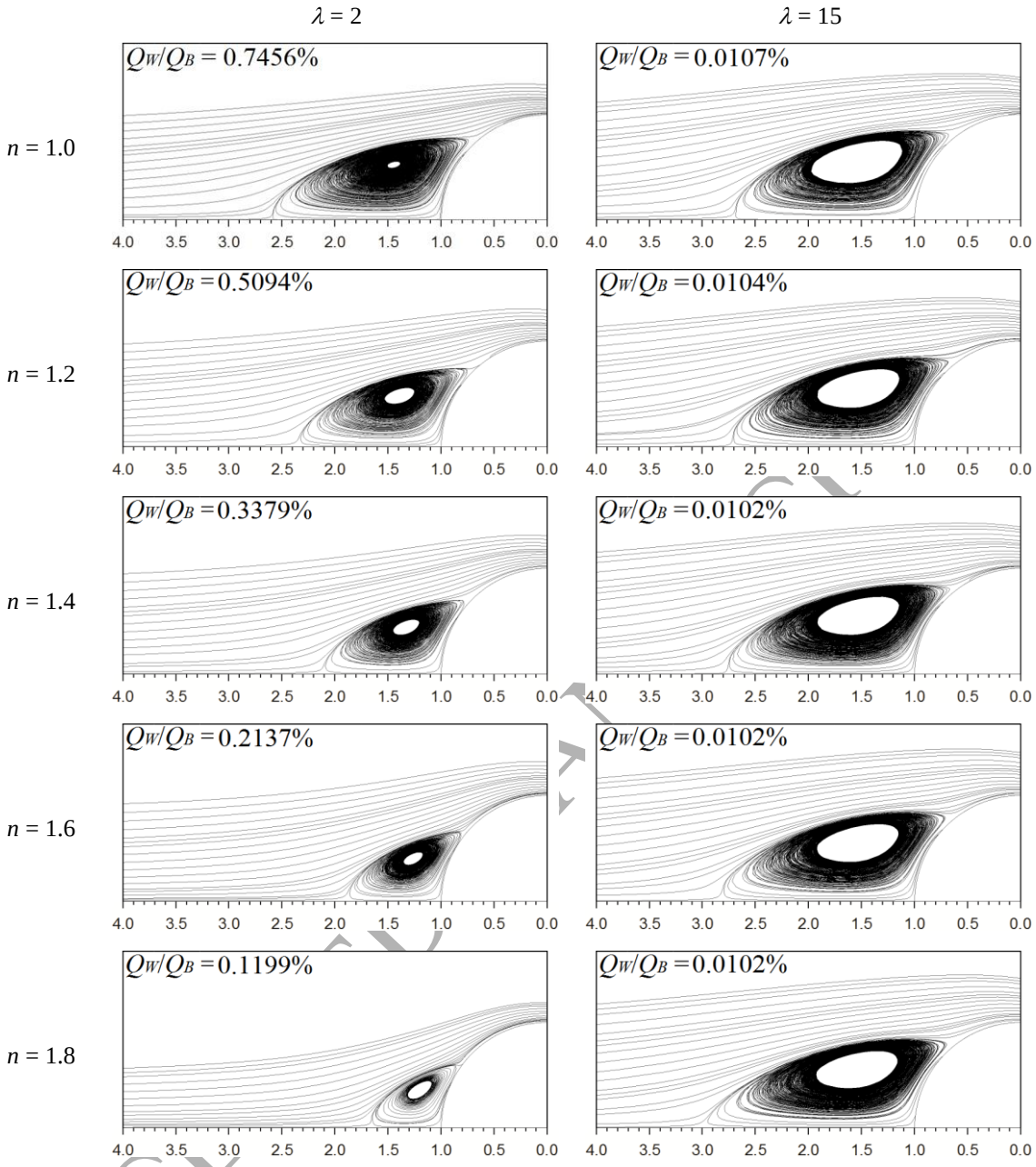

Fig. 9. Comparison of streamline patterns after the particle with different values of n for λ = 2 and 15 at Re = 100

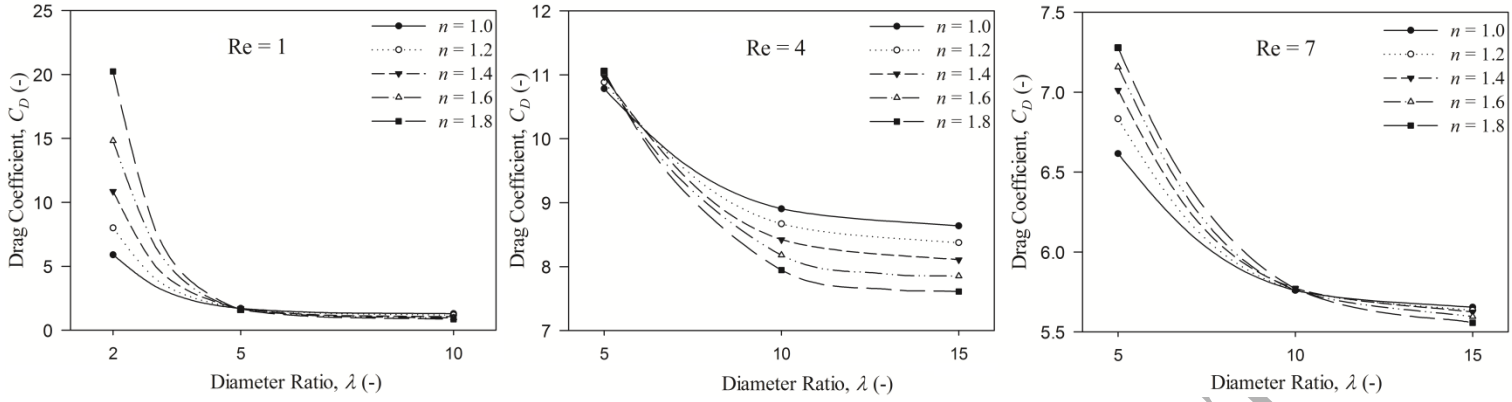

Fig. 10. Comparisons of C_D with different values of λ for Newtonian and shear-thickening power law fluids at Re = 1, 4 and 7.

Table 1. Comparisons of C_D at different values of Re in unbounded Newtonian and shear-thickening fluids.

n	Re = 0.001		Re = 0.01		Re = 1		Re = 10			Re = 100		
	Tripathi and Chhabra [23]	Present*	Tripathi and Chhabra [23]	Present*	Dhole, et al. [22]	Present*	Dhole, et al. [22]		Present*	Dhole, et al. [22]		Present*
							FVM	FDM		FVM	FDM	
1	24001.03	23890	2400.19	2389	27.15	27.47	4.28	4.34	4.31	1.06	1.09	1.09
1.2	19845.41	19580	1984.55	1959	24.16	24.24	4.52	4.42	4.41	1.26	1.25	1.24
1.4	13665.79	13640	1366.58	1366	21.27	21.49	4.62	4.47	4.48	1.41	1.40	1.37
1.6	9367.53	9287	936.76	935.3	19.43	19.21	4.72	4.52	4.52	1.57	1.55	1.50
1.8	6275.69	6201	627.57	627.5	17.08	17.34	4.85	N/A	4.55	1.69	N/A	1.62

*Extrapolation

Table 2. Comparisons of Y with different values of λ in bounded Newtonian and shear-thinning fluids for creeping flow.

n		2	5	10	15	20	50
1.0	Haberman and Sayre [28]	5.8700	1.6797	1.2633	1.1624	1.1173	1.0439
	Missirlis, et al. [31]	5.9471	1.6827	1.2672	1.1665*	1.1194	1.0464
	Present	5.9278	1.6799	1.2629	1.1627	1.1188	1.0425
0.5	Missirlis, et al. [31]	2.7411	1.5931	1.4923	1.4778*	1.4754	1.4738
	Present	2.7752	1.6086	1.5085	1.4965	1.4877	1.4847

*Interpolation

Table 3. Comparison of C_D with different values of λ in bounded Newtonian fluid at moderate values of Re.

		λ	5	10
n=1	Re=1	Wham, et al. [29]	40.476	30.599
		Rajasekhar and Kishore [33]	79.467	N/A
		Present	40.499	30.933
	Re=10	Wham, et al. [29]	4.794	3.853
		Rajasekhar and Kishore [33]	11.001	N/A
		Present	4.979	4.420
	Re=100	Wham, et al. [29]	1.087	1.016
		Rajasekhar and Kishore [33]	~2.6	N/A
		Present	1.162	1.101

Table 4. Comparison of normalised C_D with different values of λ in bounded shear-thinning fluid at moderate values of Re.

λ			2	5	10
n=0.4	Re=1	Song, et al. [32]	0.40	0.93	1.17
		Present	0.41	0.94	1.18
	Re=10	Song, et al. [32]	0.41	0.82	0.88
		Present	0.42	0.83	0.89
	Re=100	Song, et al. [32]	0.47	0.58	0.59
		Present	0.50	0.61	0.62

Table 5. Drag correction factor Y at Re = 0.001 and 100 with different values of λ and n.

	n	$\lambda = 2$	$\lambda = 5$	$\lambda = 10$	$\lambda = 15$	$\lambda = 20$	$\lambda = 50$	$\lambda = \infty$*
	1.0	5.9278	1.6799	1.2629	1.1627	1.1188	1.0425	0.9954
	1.2	7.9984	1.6718	1.1196	0.9807	0.9165	0.7994	0.7888
Re = 0.001	1.4	10.8681	1.6495	0.9722	0.8030	0.7239	0.5749	0.5683
	1.6	14.8101	1.6160	0.8302	0.6424	0.5555	0.3934	0.3870
	1.8	20.2386	1.5748	0.7002	0.5050	0.4170	0.2592	0.2584
	1.0	9.6277	4.8433	4.5856	4.5541	4.5499	4.5423	4.5440
	1.2	12.1204	5.5285	5.1951	5.1521	5.1492	5.1389	5.1320
Re = 100	1.4	15.2345	6.1998	5.7791	5.7237	5.7193	5.7064	5.7010
	1.6	19.2287	6.8496	6.3317	6.2628	6.2564	6.2395	6.2430
	1.8	24.5192	7.4741	6.8505	6.7666	6.7579	6.7371	6.7391

*Extrapolation

Table 6. Length of recirculation wakes at Re = 100 with different values of λ and n.

n	$\lambda = 2$	$\lambda = 5$	$\lambda = 10$	$\lambda = 15$	$\lambda = 20$	$\lambda = 50$	$\lambda = \infty$*
1.0	1.59r	1.66r	1.72r	1.71r	1.72r	1.72r	1.72r
1.2	1.35r	1.66r	1.73r	1.74r	1.74r	1.74r	1.74r
1.4	1.11r	1.68r	1.77r	1.75r	1.78r	1.78r	1.78r
1.6	0.88r	1.70r	1.81r	1.82r	1.83r	1.83r	1.83r
1.8	0.67r	1.78r	1.93r	1.94r	1.93r	1.94r	1.94r

*Extrapolation

Table 7. Percentage of recirculation flow rate at Re = 100 with different values of λ and n.

n	$\lambda = 2$	$\lambda = 5$	$\lambda = 10$	$\lambda = 15$	$\lambda = 20$	$\lambda = 50$
1.0	0.7456%	0.0974%	0.0241%	0.0107%	0.0057%	0.0009%
1.2	0.5094%	0.0918%	0.0231%	0.0104%	0.0056%	0.0009%
1.4	0.3379%	0.0880%	0.0227%	0.0102%	0.0056%	0.0009%
1.6	0.2137%	0.0856%	0.0226%	0.0102%	0.0056%	0.0009%
1.8	0.1199%	0.0838%	0.0227%	0.0102%	0.0056%	0.0009%